INVESTIGATION OF THE TURBULENT BOUNDARY LAYER PERTURBED BY A TRIANGULAR RIPPLE

Fernando David Cúñez Benalcázar, fernandodcb@fem.unicamp.br
Erick de Moraes Franklin, franklin@fem.unicamp.br
University of Campinas, Faculty of Mechanical Engineering, Rua Mendeleyev, 200, Campinas, 13083-970, Brazil

Abstract: *In the present study, experiments have been performed for the investigation of the perturbation of a fully-developed turbulent boundary layer by a two-dimensional hill of triangular shape. Different water flows were imposed over an asymmetric triangular hill fixed on the bottom wall of a closed conduit, and the flow field was measured by PIV (Particle Image Velocimetry). Reynolds numbers based on the channel height varied between 27500 and 35000 and the regime was hydraulically smooth. From the instantaneous flows fields, the mean velocities and fluctuations were computed, and the shear stress over the ripple could be determined. The general behaviors of obtained velocities and stresses are compared to published asymptotic analyses and the surface shear stress is discussed in terms of bed stability.*
Keywords: *Turbulence, Boundary layer, Perturbation of the boundary layer*

1. INTRODUCTION

Turbulent boundary layers over flat walls perturbed by low hills are frequently found in industry and nature and, for this reason, they have been extensively studied for ever a century. In nature, some examples are atmospheric flows over hills, ocean waves and desert dunes, and water flows over river dunes. In industry, some examples are the flows over sand ripples and dunes (which have a triangular shape) in closed conduits such as petroleum and air-conditioning pipelines. The perturbation of a two-dimensional boundary layer by a triangular ripple introduces new scales in the problem, changing the velocity and stress distributions along the flow that are of importance for many engineering applications. For example, when in the presence of sediment transport, the new distributions are essential to understand the bed instabilities.

Over the last years, many studies have been devoted to the perturbation of a two-dimensional turbulent boundary layer by a low hill (Jackson and Hunt, 1975; Hunt *et al.*, 1988; Belcher and Hunt, 1998 and Franklin and Ayek, 2013), some of them, based on asymptotic methods, have improved our knowledge on the subject. In these methods, the turbulent boundary layer perturbed by a hill of small aspect ratio (height to length ratio of $O(0.1)$) is divided into a two-region structure that can be used to determine the perturbed flow (Belcher and Hunt, 1998).

Jackson and Hunt (1975) have presented an asymptotic analysis of two-dimensional turbulent boundary layer perturbed by a low hill. In their analysis, the unperturbed boundary layer was given by the law of the wall, and they divided the perturbed boundary layer into two regions. The inner region, close to the bed, is a region where the turbulent vortices can adapt to equilibrium conditions with the mean flow. In this region, the timescale for the dissipation of the energy-containing eddies is much smaller than the timescale for their advection, so that this region is in local-equilibrium. The outer region, far enough from the bed, so that the energy-containing vortices can not adapt to equilibrium conditions with the mean flow, the timescale for the dissipation of the energy-containing eddies is much larger than the timescale for their advection, and the flow is not in local equilibrium.

Jackson and Hunt (1975) matched the inner region and the outer region and obtained a solution for the perturbation. Their composite solution shows that most of the perturbation occurs in the inner region. Hunt *et al.* (1988) also showed that the maximum od the perturbation velocity occurs in the shear stress layer. Based on Jackson and Hunt (1975) and Hunt *et al.* (1988), Weng *et al.* (1991) computed the velocity perturbations until the second order and applied the results to forms with higher aspect ratios. The proposed expressions for the surface stresses, at the first order, are largely employed. Kroy *et al.* (2002a) and Kroy *et al.* (2002b) simplified the results of Weng *et al.* (1991) for the surface stress and obtained an expression containing only the dominant physical effects of the perturbation, making clear the reasons for its upstream shift. Carruthers and Hunt (1990) showed that reasonable results are obtained for higher forms, with slopes up to 0.3.

Poggi *et al.* (2007) performed experiments on turbulent flows over a two-dimensional hilly surface. In their study, they found that within the inner region, the shear stress along the hill is approximately constant. Moreover, Franklin and Charru (2011) and Charru and Franklin (2012) studied the isolated three dimensional dunes, known as barchans, in the specific case of closed-conduit water flows. The authors found that the surface shear stress along the symmetry plane of the dune is not shifted upstream of the dune crest. If this is true, the liquid flow is not the unstable mechanism and the formation of aquatic barchans cannot be understood. The absence of an upstream shift was not explained by the authors, the reason being probably linked to the flow three-dimensionality.

In a recent work, Franklin and Ayek (2013) studied the evolution of the shear stress over a triangular profile. Their experimental results showed that the maximum of the shear stress on the ripple surface occurs upstream of the ripple crest and the flow is not in local-equilibrium conditions along the upstream face of the ripple.

This paper presents an investigation on the perturbation of a two-dimensional fully-developed turbulent boundary layer by triangular ripple. Two water flows were imposed over an asymmetric triangular hill fixed on the bottom wall of a closed conduit and the flow field was measured by PIV (Particle Image Velocimetry). From the instantaneous flow fields,

the mean velocities and fluctuations were computed. The obtained velocities and stresses are compared to published asymptotic analyses and the surface shear stress is discussed in terms of instabilities of a granular bed.

2. EXPERIMENT

The experimental device consisted of a water reservoir, two centrifugal pumps, a flow meter, a flow straightener, a *5m* long rectangular transparent channel (*160mm* wide by *50mm* high), a settling tank, and a return line, so that the water flowed in a closed loop following the above order of description. The flow straightener consisted of a divergent-convergent nozzle filled with glass spheres with a diameter of d = *3mm* whose function was to homogenize the flow profile. The channel test section was *1m* long and started at 40 hydraulic diameters (*3m*) downstream of the channel inlet. There was another *1m* long section connecting the test section exit to a settling tank and the return line. Figure 1 presents a layout of the experimental device.

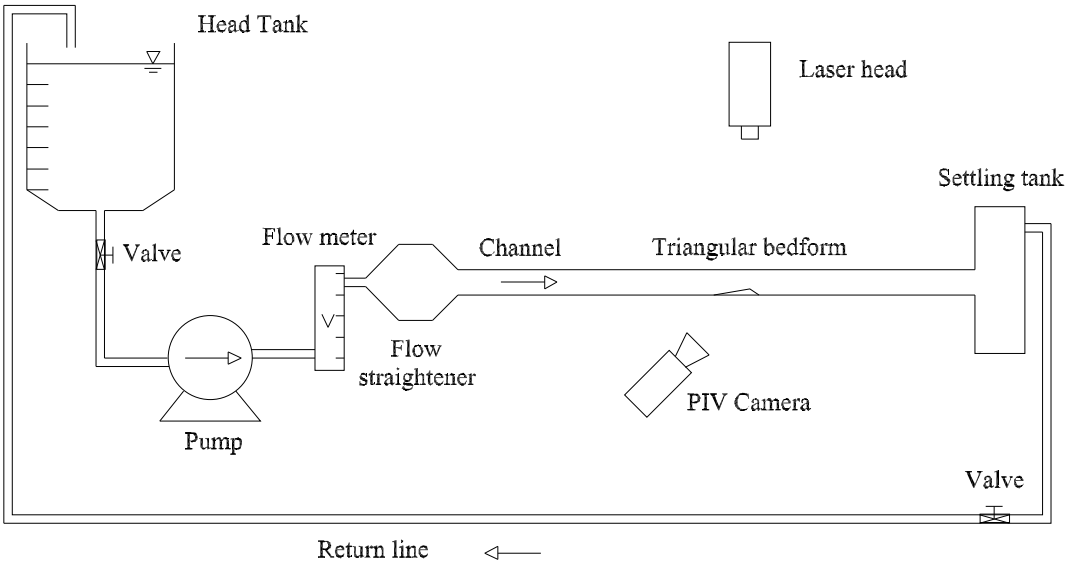

(a)

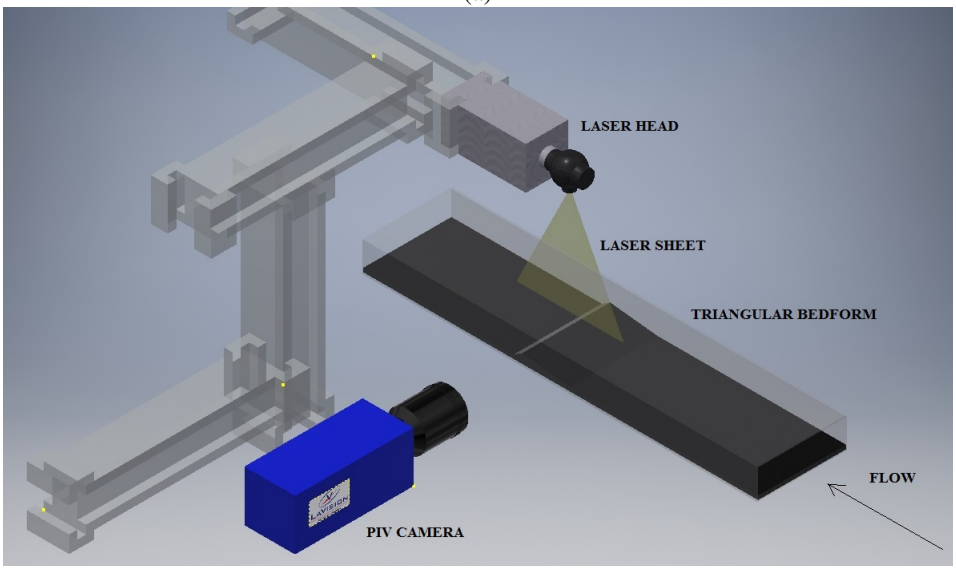

(b)

Figure 1: **Layout of the experimental device (a) Side view. (b) Test section 3D view.**

Two flow rates were employed, *8* and *10*m^3*/h*, corresponding to cross-section mean velocities $\bar{U}$ of *0.32* and *0.40m/s* and to Reynolds numbers $Re = \bar{U}2H_{eff}/\nu$ of *2.75*$\times$*10*^{4} and *3.5*$\times$*10*^{4}, respectively, where H_{eff} is the distance from the surface of the PVC plates to the top wall of the channel. The regime was hydraulically smooth in all the cases.

PVC plates of *7mm* thickness were inserted in the channel, covering its entire bottom and reducing its height. A *99.4mm* long, *9.4mm* height triangular shape model, with *6.36*° upwind angle was employed in the tests. It had the same

scales as the aquatic ripples and closed-conduit dunes, and was fixed on a PVC plate on the bottom wall of the channel in the text section (Fig.1b).

Four measurements were performed for each flow: one without the ripple and three with the ripple in test section and were taken at the vertical symmetry plane of the channel. Particle Image Velocimetry (PIV) was employed to obtain the instantaneous fields of the flow. The employed light source was a dual cavity Nd:YAG Q-Switched laser, capable to emit $2\times130mJ$ at $15Hz$ pulse rate. To capture the images we used a $7.4\mu m \times 7.4\mu m$ (px^2) CCD (charge coupled device) camera with a spatial resolution of $2{,}048px \times 2{,}048px$ and acquiring pairs of images at $4Hz$ (synchronized with the lasers). The total field employed was of $140mm \times 140mm$, the employed interrogation area was of $16px \times 16px$, and the computations were made with 50% of overlap. This corresponds to 512 interrogation areas.

$10\mu m$ diameter hollow glass beads ($S.G. = 1.05$) were employed as seeding particles. These particles required the power of the laser to be fixed at 66% of the maximum power to assure a good balance between the image contrasts and undesirable reflection from the channel walls. Each of the four experimental tests acquired 2000 pairs of images for both flow rates. Instantaneous velocity fields were computed in fixed Cartesian grids by the PIV controller software (DaVis). MatLab scripts were written to post-process these fields (time-averaged velocity, velocity fluctuations, spatio-temporal averaged profiles, shear velocities, stresses on the ripple coordinate system, for example).

3. RESULTS

3.1 Unperturbed flow

The first measurements were made without the triangular ripple, corresponding then to a turbulent, unperturbed, fully-developed channel flow. Two flow rates of 8 and $10m^3/h$ were imposed. For each test, the instantaneous fields were time-averaged and the fluctuation fields were computed and time-averaged. The time-averaged fields were then space-averaged in the longitudinal direction because the flow was fully developed.The measurements showed that the law of the wall and the Blasius correlation are valid for the turbulent flow in the test section and therefore can be used to estimate the unperturbed flow.

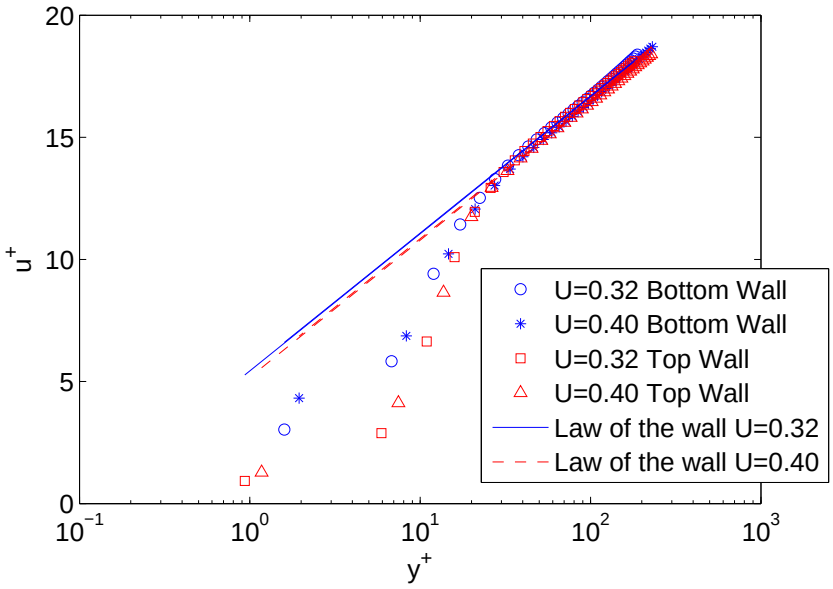

Figure 2: **Mean velocity profiles.**

Figure 2 presents the log-normal profiles of the mean velocities for two Reynolds numbers. The abscissa is in logarithmic scale and represents the vertical distance from the channel walls (bottom or top) normalized by the viscous length, $y^+=yu_*/\nu$. The ordinate is in linear scale and corresponds to the mean velocities normalized by the shear velocity, $u_0^+=u/u_{*,0}$. The shear velocity $u_{*,\circ}$ for each Reynolds number was determined by fitting the experimental data in the logarithmic region ($70 < y^+ < 200$). The corresponding values of $u_{*,\circ}$, $B_\circ$ and the Darcy friction factor $f_\circ$, as well as the symbols employed in (Fig.2), are presented in Table 1.

Table 1: **Computed shear velocity $u_{*,\circ}$, constant $B_\circ$ and friction factor $f_\circ$ for each water flow rate Q.**

$Q(m^3/h)$	$\bar{U}$	Re	$Symbol$	$B_\circ$	$u_{*,\circ}$	$f_\circ$
8	0.32	2.75×10^4	$\circ$	5.41	0.0193	0.0268
8	0.32	2.75×10^4	$\diamond$	5.93	0.0182	0.0237
10	0.40	3.50×10^4	$*$	5.16	0.0237	0.0250
10	0.40	3.50×10^4	$\triangle$	5.75	0.0227	0.0231

3.2 Perturbed flow

Two water flow rates were employed in the tests with the ripple: *8* and $10m^3/h$, that correspond to $\bar{U} = 0.32m/s$ and *0.40m/s* and to $Re = 2.75\times10^4$ and $Re = 3.5\times10^4$, respectively.

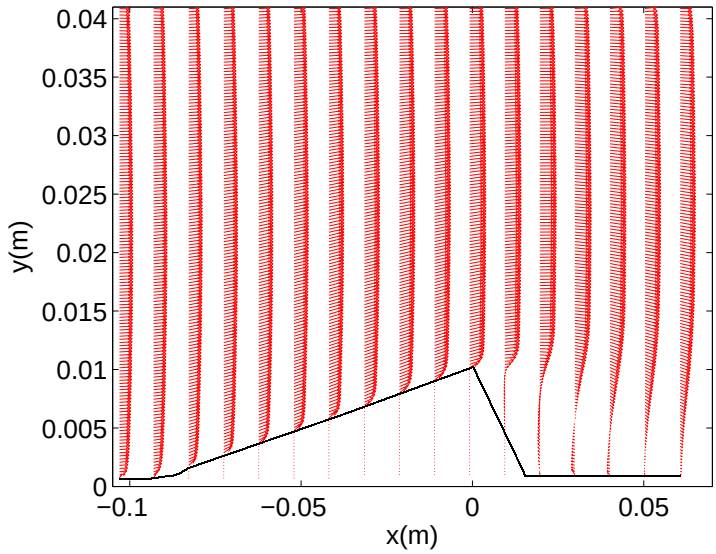

Figure 3: **Some profiles of the perturbed mean velocities over the triangular ripple. The flow is from left to right and $Re = 2.75\times10^4$.**

Figure 3 shows some mean velocity profiles $\vec{V}(y) = u(y)\vec{i} + v(y)\vec{j}$ over the triangular ripple. In Figs.3 to 9, the position $x = 0$ corresponds to the ripple crest. The main characteristics of the mean flow can be obtained from this figure, which shows that water stream is deflected by the ripple. Upstream of the crest, v is directed upward. Downstream of the crest, the flow detaches and a recirculation bubble is generated. Far from the ripple surface, the values of v are negligible. Although $v \approx 0$, the longitudinal component of the velocity u is accelerated in this region due to the confinement.

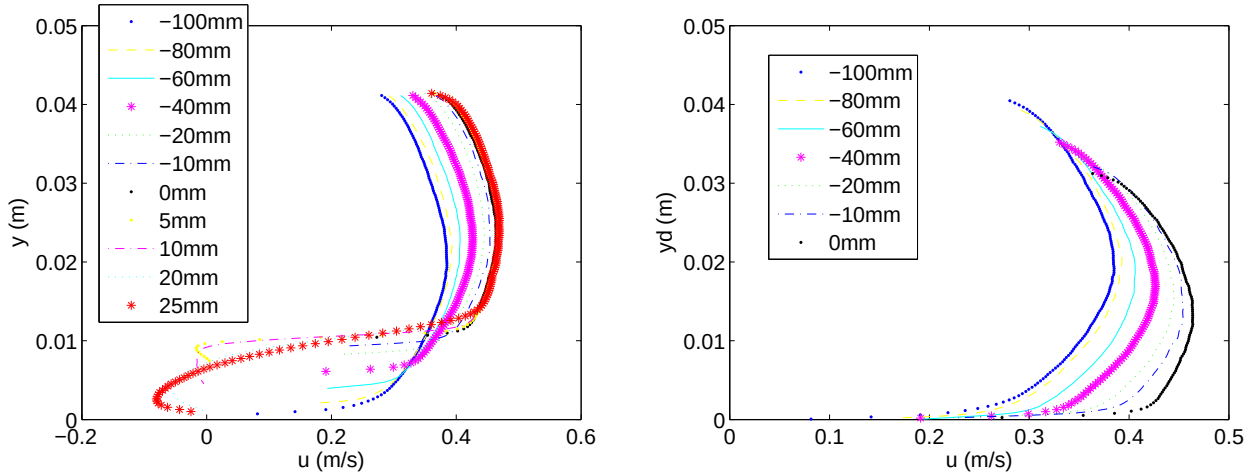

(a) (b)

Figure 4: **(a) Longitudinal component of some mean velocity profiles $u(y)$. (b) Longitudinal component of some mean velocity profiles $u(y_d)$. $Re = 2.75\times10^4$.**

Figure 4 presents the longitudinal component of some mean velocity profiles $u(y)$ over the ripple. The employed symbols correspond to the longitudinal position indicated in the legends. Fig.4a presents y versus u, being suitable for an analysis of the core flow and upper wall regions. The maximum of u does not occur at the crest ($x = 0$) because of nonlinear interactions and, due to a strong recirculation bubble and flow confinement, the core flow is affected. Fig.4b presents y_d versus u, being suitable for the analysis to the boundary layer in the lower region. In $x<0$ region, u increases as the flow approaches the crest and a great part of the perturbation is confined in the lower region. Downstream of the crest, the flow detaches and u has negative values.

The vertical displaced coordinate can be defined as:

$$y_d = y - h \tag{1}$$

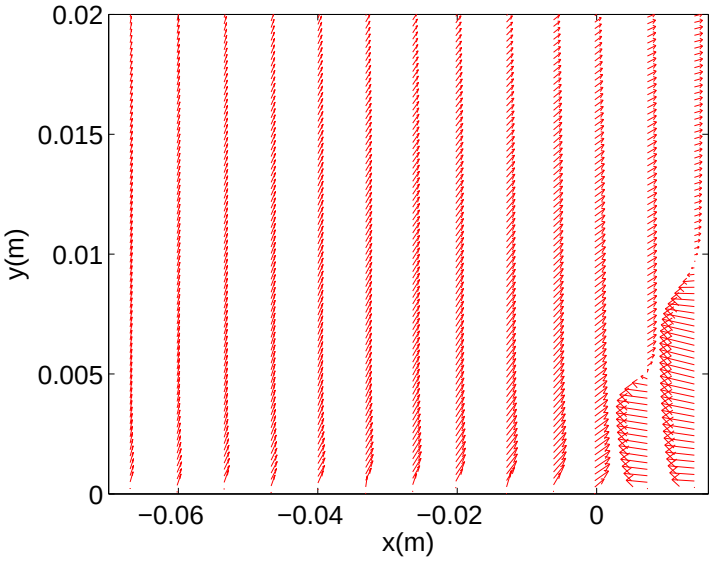

Figure 5: **Some perturbation profiles of the mean velocities *Re = 2.75×10*^{4}.**

where $h = h(x)$ is the local height of the triangular ripple and y_d is called displaced vertical coordinate.

Jackson and Hunt (1975) presented an expression to define the perturbation field as the difference between the velocity over the ripple and that unperturbed, in the displaced coordinate system. This gives:

$$\Delta\vec{V}(y_d) = \vec{V}(y_d) - \vec{V}_0(y_d) \tag{2}$$

where $\vec{V}_0(y_d)$ is the unperturbed flow. Figure 5 presents 13 perturbation profiles of the mean velocities along the ripple. Downstream of the crest, the perturbations have a negative value because the flow detaches and a recirculation bubble is generated. Upstream of the crest, the perturbations increase toward the crest and are localized in the region $y_d < 2mm$. If the displaced coordinate is normalized by the viscous length of the unperturbed flow, we obtain $y_d^+ = y_d u_*/\nu < 43$. This region is found to correspond to the buffer and viscous layers of the unperturbed boundary layer, where the viscous shear stress is very important (Schlichting, 2000).

Turbulent stresses are of importance in the layers above the viscous layer. Figure 6 presents some profiles of the *xy* aligned component of the Reynolds stresses with respect to the triangular ripple surface upstream of the ripple crest in dimensionless form, y_d^+ versus $-\overline{u'_\theta v'_\theta}/(u^2_{*,0})$. To decrease the noise, the obtained $-\overline{u'_\theta v'_\theta}$ profiles were averaged by a sliding window process over the closest nine points. If the flow is in local equilibrium in the $y_d{}^+ < 250$ region, the values of $-\overline{u'_\theta v'_\theta}$ in the overlap layer shall scale with $\tau_{visc}/\rho = u^2_*$, which in turn is expected to be a small perturbation of $\tau_0/\rho = u^2_{*,0}$. In other words, $-\overline{u'_\theta v'_\theta}$ must have the same order of magnitude as $u^2_{*,0}$ to be in local equilibrium. Figure 6 also shows that, longitudinally, the perturbation of $-\overline{u'_\theta v'_\theta}$ decreases near the crest.

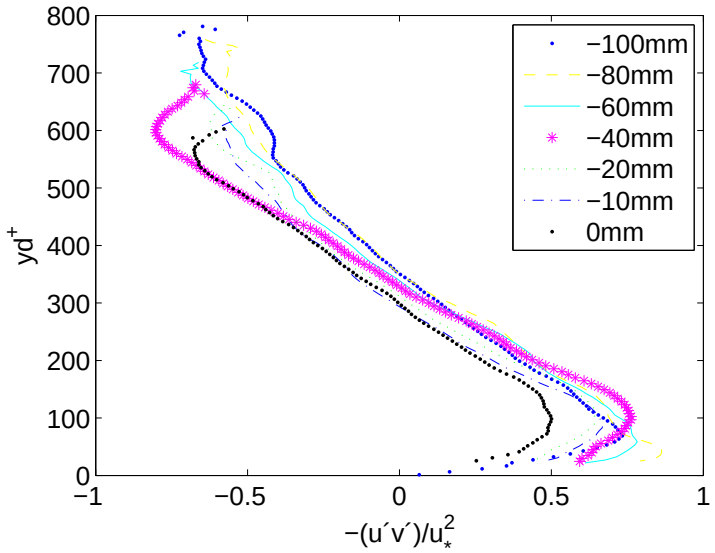

Figure 6: **Some profiles of the Reynolds stress *xy* aligned component in dimensionless form upstream of the triangular ripple crest: $y_d{}^+$ versus $-\overline{u'_\theta v'_\theta}/(u^2_{*,0})$. *Re = 2.75×10*^{4}.**

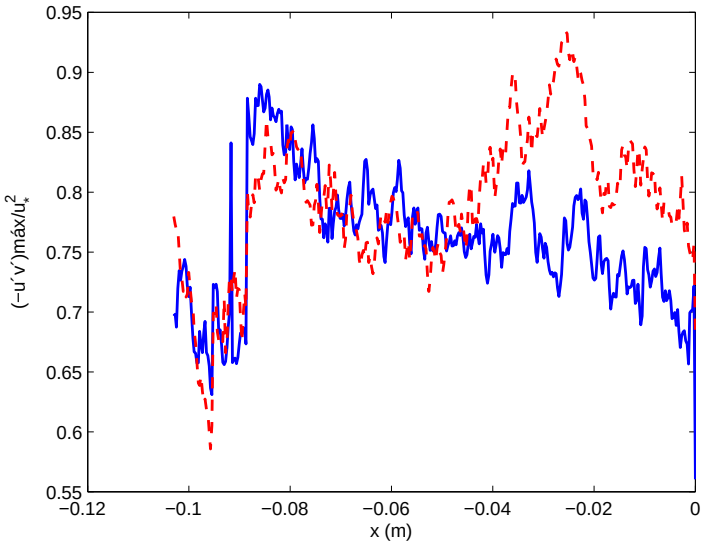

Figure 7: **Maximum normalized Reynolds stress ($\text{-}\overline{u'_\theta v'_\theta})_{max}/(u_{*,0}{}^2$) as a function of the longitudinal position *x*. The *continuous* and *dashed lines* correspond to *Re* = 2.75×10^4 and *Re* = 3.5×10^4, respectively.**

Figure 7 presents the longitudinal evolution of the maximum of the *xy* Reynolds stress $(\text{-}\overline{u'_\theta v'_\theta})_{max}$ (for each vertical profile) normalized by $u^2_{*,0}$, for the bottom wall region. In this figure, the continuous and dashed lines correspond to *Re* = 2.75×10^4 and *Re* = 3.5×10^4 ($\bar{U}$ = *0.32 and 0.4 m/s*), respectively. Figure 7 shows that $(\text{-}\overline{u'_\theta v'_\theta})_{max}$ increases approximately *20%* where the triangular ripple starts at $x \approx$ *-0.09m*. For *Re* = 2.75×10^4, $(\text{-}\overline{u'_\theta v'_\theta})_{max}$ decreases in the $0.09m \leq x \leq 0m$ region until $(\text{-}\overline{u'_\theta v'_\theta})_{max} \approx 0.65\ u^2_{*,0}$. For *Re* = 3.5×10^4, $(\text{-}\overline{u'_\theta v'_\theta})_{max}$ has a different behavior in the $0.09m \leq x \leq 0m$ region, but this cannot be asserted because of the relatively high noise in the data. However we obtain that $(\text{-}\overline{u'_\theta v'_\theta})_{max} \sim O(u^2_{*,0})$ (for each case) in the region analyzed. It seems to us that the flow is in local-equilibrium because in the upstream region $\text{-}\overline{u'_\theta v'_\theta}$ has the same order of magnitude that $u^2_{*,0}$.

To understand if the water flow is an unstable mechanism and if the flow is in local equilibrium within ($0 < y_d^+ < 250$), the viscous shear stress on the ripple surface τ_{visc} is of interest and was evaluated as:

$$\tau_{visc} \approx \mu \frac{\partial u_\theta}{\partial y_{d,\theta}} \tag{3}$$

where u_θ is the aligned component of the mean velocity with respect to the triangular ripple surface and $y_{d,\theta}$ is a displaced coordinate perpendicular to the ripple surface.

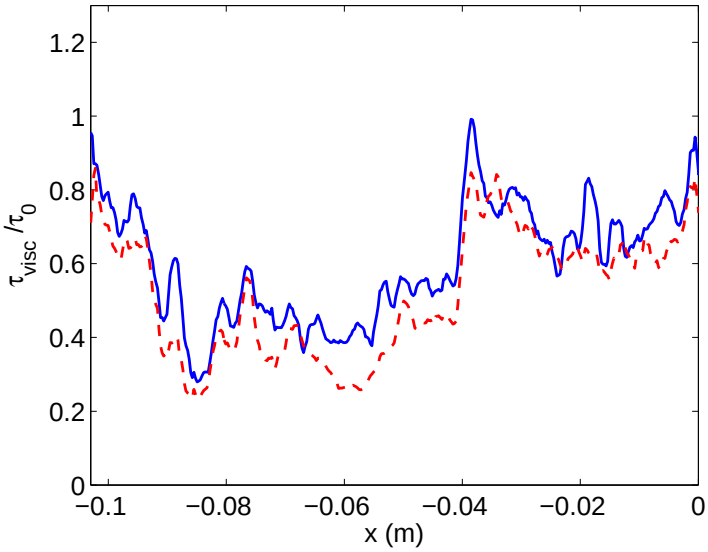

Figure 8: **Normalized surface viscous stress τ_{visc}/τ_0 as a function of the longitudinal position *x*. The *continuous* and *dashed lines* correspond to *Re* = 2.75×10^4 and *Re* = 3.5×10^4, respectively.**

Figure 8 presents the evolution along the ripple of the surface viscous stress τ_{visc} normalized by the unperturbed shear stress $\tau_0 = \rho u^2_{*,0}$. Based on the unperturbed measurements (Tab. 1), the unperturbed shear stress was evaluated from the

Blasius correlation. From this figure, it seems that the maximum of the surface stress occurs upstream of the ripple crest. In this figure, the continuous and dashed lines correspond to $Re = 2.75\times10^4$ and $Re = 3.5\times10^4$ ($\bar{U} = 0.32$ *and* 0.4 *m/s*), respectively.

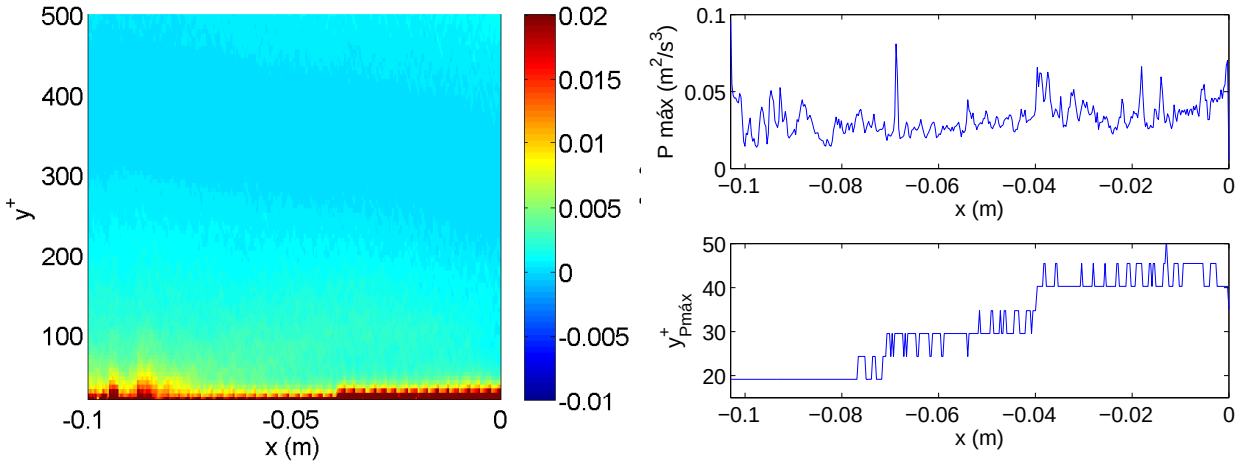

(a) (b)

Figure 9: **(a) Production of turbulence upstream of the triangular ripple crest in adimensional displaced vertical coordinate y_d^+. (b) Longitudinal evolution of Production of turbulence and $y_{d\,Pmax}^+$. $Re = 2.75\times10^4$.**

Figure 9 a) shows the production of turbulence upstream the ripple crest in the dimensionless form of the displaced vertical coordinate y_d^+, and $Re = 2.75\times10^4$. This term is calculated by:

$$P = -(\overline{u'_\theta v'_\theta})\frac{\partial u_\theta}{\partial y_{d,\theta}} \tag{4}$$

where -$(\overline{u'_\theta v'_\theta})$ is each profile of the xy aligned component of the Reynolds stresses from the ripple starts toward the crest, u_θ is the aligned component of the mean velocity with respect to the triangular ripple surface and $y_{d,\theta}$ is a displaced coordinate perpendicular to the ripple surface.

Figure 9 b) presents the longitudinal evolution of maximum value of the production of turbulence and the position in the dimensionless form of the displaced vertical coordinate where P_{max} occurs for each profile. From Fig. 9 b), we observe that the maximum value of the production of turbulence occurs in the ($y_d^+ < 50$) region, that corresponds to the buffer and viscous layers of the unperturbed boundary layer.

4. CONCLUSIONS

This paper studied the turbulent boundary layer perturbed by a low triangular ripple in the hydraulic smooth regime. The experiments were performed in moderate Reynolds numbers *(25,000<Re<35,000)*.

The water flow was measured by PIV and the obtained mean and turbulent fields were compared with unperturbed flow fields. The xy component of the turbulent stress was computed and profiles of -$\overline{u'v'}$ over the triangular ripple were found. These profiles were compared with the square of the unperturbed shear velocity $u_{*,0}^2$.

For the unperturbed flow, we found that the profiles follow the law of the wall, with a well-defined logarithmic region ($70 < y^+ < 200$). This justifies the hydraulic smooth assumption and indicates that the shear velocities $u_{*,0}^2$ for each experiment were determined correctly.

The main features of the perturbed turbulent boundary layer over a low ripple were confirmed by the experimental results shown in Fig.3: A recirculation bubble is formed downstream of the ripple crest. Also the perturbation profiles of the mean velocities $\Delta\vec{V}(y_d)$ along the ripple indicate that the perturbation increases slightly from the ripple leading edge toward the crest, in a region found to the buffer and viscous layers of the unperturbed boundary layer.

Along the upstream face of the ripple, the maximum value of the turbulent stresses are of the same order of magnitude of the square of the unperturbed shear velocity. In addition, the surface viscous stresses τ_{visc} are of the same order of magnitude of the unperturbed shear stress $\tau_0 = \rho u_{*,0}^2$. Based on these characteristics, it seems that the flow is in local equilibrium in the upstream ripple region for each experiment.

The maximum of the production turbulence along the ripple was located in the ($y_d^+ < 50$) region. For $Re = 2.75\times10^4$, $(-\overline{u'v'})_{max}$ decreases in the $0.09m \leq x \leq 0m$ region until $(-\overline{u'v'})_{max} \approx 0.65\ u_{*,0}^2$, and in this region the flow is in local-equilibrium allowing the use models for turbulent stresses.

5. ACKNOWLEDGEMENTS

Fernando David Cúñez Benalcázar is grateful to SENESCYT (Programa de Becas Convocatoria Abierta 2014 Segunda Fase), Erick de Moraes Franklin is grateful to FAPESP (grant no. 2012/19562-6) and to CNPq (grant no. 471391/2013-1)

for the provided financial support.

6. REFERENCES

Belcher, S.E. and Hunt, J.C.R., 1998. "Turbulent flow over hills and waves". Vol. 30, pp. 507–538.

Carruthers, D.J. and Hunt, J.C.R., 1990. "Fluid mechanics of airflows over hills: turbulence, fluxes, and waves in the boundary layer". *Atmospheric Processes over Complex Terrain*, Vol. 23, pp. 83–108.

Charru, F. and Franklin, E.M., 2012. "Subaqueous barchan dunes in turbulent shear flow. part 2. fluid flow". *Journal of Fluid Mechanics*, Vol. 694, pp. 131–154.

Franklin, E.M. and Ayek, G.A., 2013. "The perturbation of a turbulent boundary layer by a two-dimensional hill". *Journal of the Brazilian Soc. Mechanical Sciences*, Vol. 35, pp. 337–346.

Franklin, E.M. and Charru, F., 2011. "Subaqueous barchan dunes in turbulent shear flow. part 1. dune motion". *Journal of Fluid Mechanics*, Vol. 675, pp. 199–222.

Hunt, J.C.R., Leibovich, S. and Richards, K., 1988. "Turbulent shear flows over low hills". *Quart. J. R. Met. Soc.*, Vol. 114, pp. 929–955.

Jackson, P.S. and Hunt, J.C.R., 1975. "Turbulent wind flow over a low hill". *Quart. J. R. Met. Soc.*, Vol. 101, pp. 1435–1470.

Kroy, K., Sauermann, G. and Herrmann, H.J., 2002a. "Minimal model for aeolian sand dunes". Vol. 66, No. 031302.

Kroy, K., Sauermann, G. and Herrmann, H.J., 2002b. "Minimal model for sand dunes". Vol. 88, No. 054301.

Poggi, D., Katul, G., Albertson, J. and Ridolfi, L., 2007. "An experimental investigation of turbulent flows over a hilly surface". *Physics of Fluids (1994-present)*, Vol. 19, No. 3, p. 036601.

Schlichting, H., 2000. *Boundary layer theory*. Springer.

Weng, W.S., Hunt, J.C.R., Carruthers, D.J., Warren, A., Wiggs, G.F.S., Livingstone, I. and Castro, I., 1991. "Air flow and sand transport over sand-dunes". pp. 1–21.

7. RESPONSIBILITY NOTICE

The author(s) is (are) the only responsible for the printed material included in this paper.